ELSEVIER

Journal of Hydrology 243 (2001) 101–119

Journal of Hydrology

www.elsevier.com/locate/jhydrol

On the structure of soil moisture time series in the context of land surface models

J.D. Albertson[a,*], G. Kiely[b]

[a]*Department of Environmental Sciences, University of Virginia, Charlottesville, VA 22903, USA*
[b]*Department of Civil and Environmental Engineering, University College Cork, Ireland*

Received 22 May 2000; revised 31 October 2000; accepted 8 November 2000

Abstract

Root-zone soil moisture is addressed as a key variable controlling surface water and energy balances. Particular focus is applied to the soil moisture controls on wet-end drainage and dry-end transpiration, and the integrated effects of these controls on the structure of soil moisture time series. Analysis is centered on data collected during a pair of field experiments, where a site in Virginia (USA) provides evidence of dynamics under dry conditions and a site in Cork (Ireland) captures dynamics under wet conditions. It is demonstrated that drainage processes (controlled by the saturated hydraulic conductivity) determine the magnitude of soil moisture at the start of the drying process and hence affect uniformly the entire distribution of soil moisture, from wet to dry. Therefore, stationary bias between predicted and measured soil moisture can be evidence of a bias in the saturated conductivity. In contrast to this, the dry-end soil controls on transpiration affect predominantly the dry-end of the soil moisture distribution, as subsequent storms act to reset the system and remove the memory of the dry state. Hence, analysis of departure between predicted and measured soil moisture that is local to the dry-end can guide estimation of the soil moisture level at which transpiration becomes limited by water availability. The temporal statistics of soil moisture are shown to exhibit threshold response to the specification of saturated conductivity in land surface models. Finally, we demonstrate the relative influences of saturated conductivity and precipitation intensity on the structural features of the root-zone soil moisture distribution.

Keywords: Root-zone; Soil moisture; Land surface models; Data Assimilation; Land-atmosphere interaction

1. Introduction

The temporal structure of soil moisture is a key feature of hydrologic interactions with climate (Entekhabi et al., 1996; Delworth and Manabe, 1988, 1989; Rodriquez-Camino and Avissar, 1998). The effects are bi-directional: vegetation and soils, through their controls on transpiration and drainage, leave a distinct imprint on the temporal structure of soil moisture (Kim and Ek, 1995; Famiglietti et al., 1998, 1999); and, over long time periods, the governing role that soil moisture plays on the partitioning of energy at the land surface manifests itself as a regional regulation on climate (Delworth and Manabe, 1989; Henderson-Sellers, 1996; Kim and Stricker, 1996; Rodriquez-Iturbe et al., 1999).

The need to predict the evolution of land surface moisture and temperature states through the course of an atmospheric forecasting model run led to the advent of land surface models (LSMs), also referred

* Corresponding author. Tel.: +1-804-924-7241; fax: +1-804-982-2137.

E-mail address: albertson@virginia.edu (J.D. Albertson).

0022-1694/01/$ - see front matter
PII: S0022-1694(00)00405-4

to as soil–vegetation–atmosphere-transfer (SVAT) models. In fact, this need spawned a wide array of competing models (see Henderson-Sellers et al., 1996). The models have enjoyed extensive application as tools in operational meteorological forecasting models, operational hydrological forecasting models, and studies of the interaction between land surfaces and atmospheric properties (e.g. Avissar and Peilke, 1991; Ek and Cuenca, 1994; Boulet et al., 1997; Belair et al., 1998).

Interesting aspects of these emerging uses relate to increasing spatial coverage and greater temporal range. These aspects demand that a model be capable of handling very different hydrologic regimes, both spatially, as found in a large forecasting model domain that might include both arid and humid regions, and temporally, as long integrations demand that runoff and drainage processes be treated robustly, such that long-term mass balances are satisfied (Kim and Stricker, 1996). Early LSM structures (e.g. Noilhan and Planton, 1989) did not universally include drainage processes. This was not an immediate problem, perhaps, for several day weather forecasts, but it is clearly unacceptable for long time integrations (Kim and Stricker, 1996). Furthermore, there is a gap between the necessary distributed applications using largely uncertain parameter sets and validation studies based on a single, heavily instrumented site.

The assessments of model performance have yielded mixed results (Chen et al., 1996; Shao and Henderson-Sellers, 1996), even at well-instrumented sites. Also, the recognition that poor performance of land surface flux estimation leads to poor atmospheric forecasts has prompted the initiation of extensive model comparison/validation exercises, such as the Project on Intercomparison of Land Surface Parameterization Schemes (PILPS) (Henderson-Sellers et al., 1993). Early results from PILPS showed a wide range in predicted water and energy balances (Henderson-Sellers et al., 1996). These findings for off-line comparison at a single well-instrumented site raised serious questions about the general utility of such models when applied over large un-instrumented regions, and ultimately the entire planetary surface. A common strategy for improving performance of individual models has been to add additional parameters, hence increasing model complexity. This is a questionable approach given that the models are to be applied over regions with a paucity of field data.

There does appear to be reason for hope for success through focused attention on key processes and perhaps a simplification rather than a further complication of model structure. Koster and Milly (1997) studied the wide disparity in model predictions and found the bulk of the differences among water and energy balances to be related to two key functional relationships: soil moisture control on evapotranspiration, and soil moisture control on runoff and drainage. In the absence of intensive field data, the water-stress thresholds and parameters describing soil controls on drainage are typically estimated from published values for representative sites (see Kim and Stricker, 1996).

Hence, we can conclude that: (i) accurate prediction of soil moisture time series is necessary to predict water and energy fluxes across the land surface, (ii) the root-zone soil moisture is most critical over vegetated regions, (iii) the dominant sources of errors in predicting time series of soil moisture are dry-end controls on evapotranspiration and wet-end controls on drainage, and (iv) there is need for approaches to identify parameters describing these functional controls for distributed areas with minimal field data.

We seek here to demonstrate the unique impacts of these key processes, drainage and transpiration, on structural features of root-zone soil moisture time series. By understanding the connection between each process and the structural features that it affects, we explore means to quantify the functional controls (parameters) on dry-end transpiration and wet-end drainage. We accomplish this using experimental field data analyzed in the context of a simple and general model structure. This provides isolation and study of impacts from individual processes. In particular, we explore soil moisture time series from field measurements at a relatively dry North American site and from a relatively wet European site.

2. Objectives

The general objectives of this paper are: (i) to illustrate the impact of transpiration and drainage controls on the structure of soil moisture time series, and (ii) to demonstrate, from a joint comparative analysis of

measured and modeled soil moisture time series, a framework for identifying the functional control of soil moisture status on evapotranspiration and drainage loses. For relevance to ungaged sites, with the future potential for remote sensing of soil moisture (e.g. Verhoest et al., 1998), we restrict our use of field data to time series of soil moisture. From these limited data sets, we seek a robust means to accurately identify the effective saturated hydraulic conductivity and the effective soil moisture threshold at which transpiration becomes water-limited.

3. Methods

We use data from two field sites and explore the measured time series in tandem with modeled time series, derived from simple conservation of mass principles.

3.1. Experiments

Observations of soil moisture dynamics under water-limited conditions are taken from a field experiment in Virginia and observations under wetter conditions are taken from measurements near Cork, Ireland. An experiment was conducted on a grass covered field at the Virginia Coastal Reserve Long Term Ecological Research Site (VCR/LTER) during the summer and fall of 1998. The experimental field was gently sloping, had ample fetch for micrometeorological measurements, and had been fallow for several years prior to and including the measurement period. On the basis of textural analysis, the soil was classified as a sandy loam (Murray, 2000). The vegetation is dominated by Johnson grass. The vegetation height ranged from 30 to 60 cm and the root zone was estimated to be 60 cm deep.

In this paper we make use of VCR/LTER measurements made on and below a 3-m micrometeorological mast, including soil moisture using time domain reflectometry (TDR) probes (Campbell CS615) at depths of 15 and 45 cm, soil temperature (Campbell 107B), soil heat flux (Campbell HFT), net radiation (Rebs Q7.1), wind speed (Campbell CSAT3), radiometric surface temperature (Everest IRT), air temperature and relative humidity (Vaisala HMP35C), precipitation (Texas Instr. tipping bucket), and sensible heat flux by eddy correlation (CSAT3). All values were averaged over 30-min periods and recorded on a Campbell 23X datalogger. The combination of the measurement period being during a significant drought on the east coast of the US and the site having fairly well-drained soils gave rise to persistantly low soil moisture levels.

Observations of wet hydroclimatic conditions are taken from a field experiment in the area of Dripsey, in County Cork, Ireland. The experimental field site is an agricultural grassland which slopes gently (1–3% grade) and has an area of 14.5 Ha. The runoff (surface and subsurface) from the site feeds a small stream at the base of the experimental field. A humus topsoil of 15 cm depth overlays a subsoil of sandy gravel, classified from detailed laboratory analysis. The grass height varies through the year from 5 to 40 cm and the root zone was determined to be 30 cm deep from soil profile analysis. The depth to water table varies through the year from 0.8 to 2 m.

Hydrological and meteorological variables were measured continuously at this site and recorded at 20 min averaging time. A tipping bucket rainguage (Obsermet OMC 400) continuously recorded rainfall. A 3-m high micrometeorological mast with a Campbell CR10X datalogger included the following sensors: an air temperature and humidity sensor (Vaisala HMP45C); a wind speed and wind direction monitor (RM Young 05103); a barometric pressure sensor (CS105); a net radiation sensor (Q7.1); a soil heat flux sensor (Campbell HFT); a soil temperature sensor (Campbell 107B) and nine soil moisture TDR probes (Campbell CS615). The soil moisture sensors are installed horizontally between the depths of 2 and 60 cm.

3.2. Model framework

There is considerable diversity in the full treatment of energy and moisture fluxes and dynamics of state variables across the range of published LSM structures. This study is not related to model development, or even model validation, but simply focuses on a single state variable (root-zone soil moisture) and the isolation of impacts from two key processes (evapotranspiration and drainage). As we noted, Koster and Milly (1997) identified the variable treatment of these processes as the greatest source of discrepancies between LSM formulations. The

prognostic equations for root-zone soil moisture (θ_{rz}) are typically more uniform across LSM formulations than are the equations for surface moisture. Hence, we can handle the evolution of θ_{rz} with a simple one-dimensional implementation of mass conservation while maintaining generality and relevance to many model structures. We account for the fluxes into and out of the root zone using conventional and simple formulations, such that cause–effect relationships are easily deduced and the results are readily adapted to other sites in the absence of detailed flux data.

The root-zone soil moisture evolves because of an imbalance between fluxes across its upper and lower boundaries

$$\frac{\partial \theta_{rz}}{\partial t} = \frac{1}{d_{rz}}\left(P_g - \frac{E_g}{\rho_\theta} - \frac{E_{tr}}{\rho_\theta} - q_{rz}\right) \tag{1}$$

where P_g is the precipitation infiltrating into the soil, E_{tr} is the transpiration rate, E_g is the soil evaporation rate, and q_{rz} is the rate of drainage out the bottom of the root-zone soil column, with the physical parameters being the density of liquid water (ρ_θ) and the depth of the root zone (d_{rz}).

Early LSM structures omitted considerations of drainage (e.g. Noilhan and Planton, 1989). However, the addition of the drainage term to Eq. (1) is critical, and also the redefinition of P_g from its historic definition as throughfall to its present definition as infiltrated-throughfall can be important in areas that experience ponding or surface runoff (Kim and Stricker, 1996). Without the drainage term, integrations of this mass conservation equation (1) over long time scales would have total evapotranspiration basically equal to total precipitation (Mahfouf and Noilhan, 1996).

The evaporation and transpiration fluxes are computed from aerodynamic exchange equations (Brutsaert, 1982), subject to the atmospheric forcing time series of incoming shortwave radiation ($R^{\downarrow}_{sw}$), air temperature (T_a), relative humidity (rh), and wind speed (U). Here we integrate the model in an "off-line" manner, where measured values of $R^{\downarrow}_{sw}$, T_a, rh, U, and P from the field experiments are used. Since we are concerned with vegetated areas, we are primarily interested in θ_{rz}, which is the state variable that affects the plants' water use and controls the rate of drainage. The surface temperature, surface moisture, deep temperature, and all energy fluxes were also provided by the full model (with a structure similar to Noilhan and Mahfouf, 1996); however, these portions of the model are not reviewed here as they are tangential to the results presented for θ_{rz}. This allows focus on the evolution of root-zone integrated soil moisture as controlled by conservation of mass. By focusing on a rigorously defined depth-averaged quantity

$$\theta_{rz} = \frac{1}{d_{rz}}\int_0^{d_{rz}} \theta(z)\,\mathrm{d}z \tag{2}$$

we can objectively compare it to field measurements of soil moisture integrated over the same depth.

The evaporation from exposed soil has a relatively minor impact on root-zone soil moisture, since $E_{tr} \gg E_g$ over well-vegetated sites as addressed here. The transpiration flux of water from the root zone is estimated as

$$\begin{aligned} E_{tr} &= f_v S \beta (1-\delta) E_{tr}^{max} \\ E_{tr}^{max} &= \rho_a (q_s^* - q_a)((C_s U)^{-1} + r_{s,min})^{-1} \end{aligned} \tag{3}$$

where f_v is the fractional vegetation cover ($0 \le f_v \le 1$), S is a seasonal index of greenness going from 0 (or some residual value) in the winter, transitioning to 1 in the spring, constant at 1 in the growing season, and decaying back to the dormant value during the fall (the dates defining the beginning and end of the spring and fall transition periods are set from regional observations), β captures the effect of soil moisture on transpiration ($0 \le \beta \le 1$) as described below, δ is the fraction of vegetation water loss coming from the interception reservoir (after Deardorff, 1978), ρ_a is the density of air, C_s ($= k^2(\ln(z/z_o) - \psi_m(\zeta))^{-1} \times (\ln(z/z_{os}) - \psi_s(\zeta))^{-1}$) is a turbulent scalar exchange coefficient accounting for surface roughness and atmospheric stability, k ($= 0.4$) is the von Karman constant, z_o is the momentum roughness height, z_{os} is the scalar roughness height, ψ_m is the stability correction for momentum, ψ_s is the stability correction for scalars, ζ is the Monin–Obuhkov stability parameter (these functions are after Brutsaert, 1982), U is the mean wind speed at height z, q_s^* is the saturated specific humidity at the ground surface temperature (T_s), q_a is the air specific humidity calculated from rh and q_a^* at T_a (Brutsaert, 1982), and $r_{s,min}$ is the minimum stomatal resistance of the vegetation (Avissar

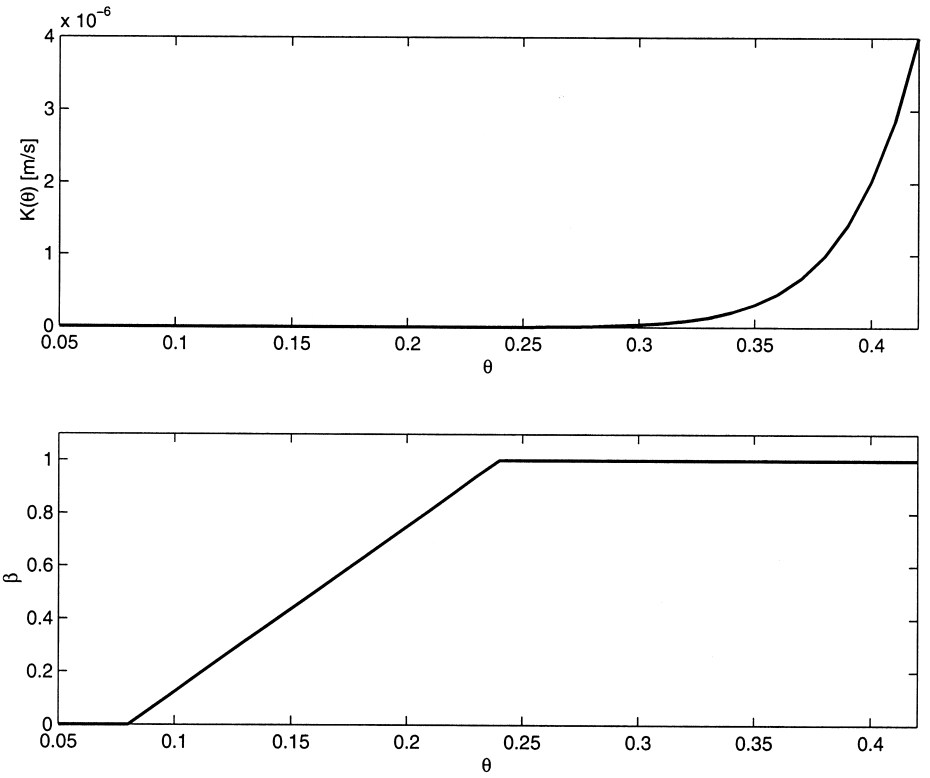

Fig. 1. The top panel shows the hydraulic conductivity ($K(\theta)$) plotted against soil moisture status, using the soil type of the Virginia site as an example. The bottom panel shows the reduction factor applied to transpiration from soil moisture status. Note that in this example $\theta_{lim} = 0.24$ and $\theta_{wilt} = 0.08$.

and Peilke, 1991; Ben-Mehrez et al., 1992). Drainage from the root zone is estimated with the assumption of a unit head gradient across the bottom of the root zone applied to Darcy's law (Kutìlek and Nielsen, 1994), such that $q_{rz} = K(\theta_{rz})$, where K is the hydraulic conductivity evaluated at the root-zone soil moisture. This is in contrast to the Newtonian restoring term used for q_{rz} by Mahfouf and Noilhan (1996), which makes use of the unit-gradient assumption but yields a more complicated formulation.

The drainage formulation we adopt is uniquely defined by the relationship between hydraulic conductivity and soil moisture status, which is simply defined based on the soil. Here, we use the Clapp and Hornberger (1978) formulation for unsaturated conductivity, with the unit-gradient assumption,

$$q_{rz} = K(\theta_{rz}) = K_{sat}\left(\frac{\theta_{rz}}{\theta_{rz,max}}\right)^{2b+3} \tag{4}$$

where K_{sat}, $\theta_{rz,max}$, and b are soil-specific hydraulic properties, possibly derived from textural information (Cosby et al., 1984).

The transpiration dependence on soil moisture is accounted for by a direct E_{tr} reduction term

$$\beta = \beta(\theta_{rz}) = \begin{cases} 0, & \text{for } \theta_{rz} \leq \theta_{wilt} \\ \dfrac{\theta_{rz} - \theta_{wilt}}{\theta_{lim} - \theta_{wilt}}, & \text{for } \theta_{wilt} < \theta_{rz} < \theta_{lim} \\ 1, & \text{for } \theta_{rz} \geq \theta_{lim} \end{cases} \tag{5}$$

where θ_{lim} and θ_{wilt} are parameters that define the states at which soil moisture becomes limiting and eventually causes vegetation to wilt and transpiration to cease, respectively (Jacquemin and Noilhan, 1990; Avissar and Peilke, 1991). We choose this simple two-parameter, piece-wise linear approach as it is parsimonious and attractive in the absence of detailed

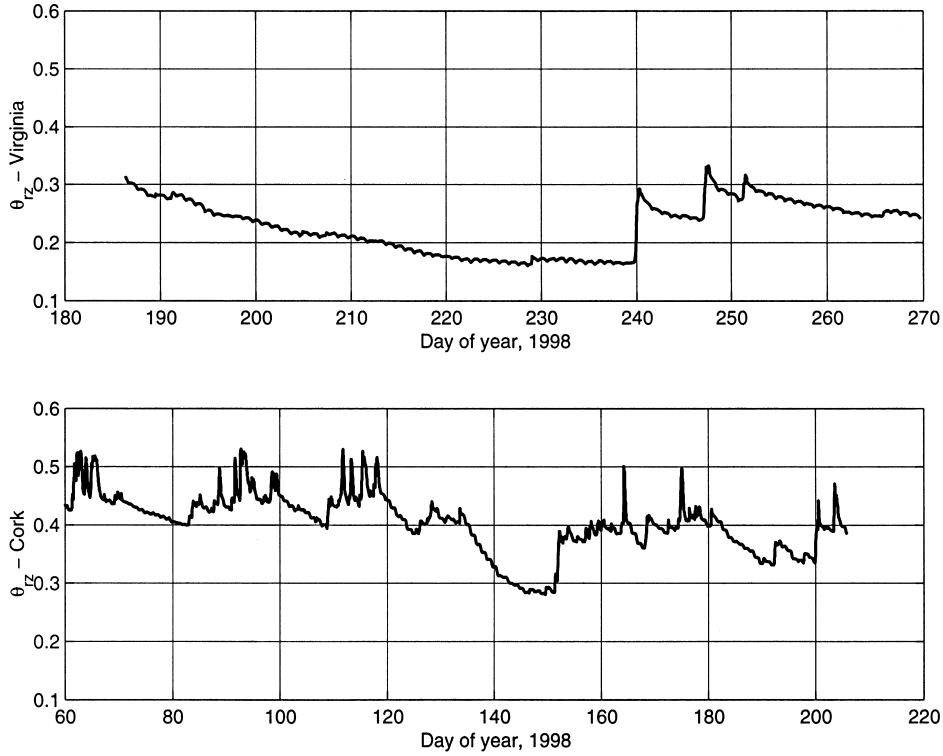

Fig. 2. Measured time series of root-zone soil moisture (θ_{rz}) at the Virginia field site (top) and the Cork field site (bottom).

information, which is the case for most SVAT applications in distributed large-scale models.

We display graphically the relationships of Eqs. (4) and (5) against soil moisture status in Fig. 1. Note that the drainage (e.g. $K(\theta)$) decreases by orders of magnitude between saturation and $\theta = 0.3$. Note also how the positions of θ_{lim} and θ_{wilt} inject controls into the transpiration process.

If Eqs. (4) and (5) impact the structure of the predicted soil moisture time series in distinctly different ways, then it should be possible to identify the parameters in Eqs. (4) and (5) from comparisons of measured and predicted soil moisture. This is accomplished by focusing on particular attributes of the time series affected uniquely by an individual process. We seek to identify this information solely from soil moisture observations, without resort to flux measurements since these are unavailable over most locations.

Typical uncertainties in K_{sat} have a greater impact on the $K(\theta)$ versus θ curve than do typical uncertainties in b; hence, we study impacts of K_{sat} in Eq. (4) on the θ_{rz} time series. If we consider that nearly all drainage occurs during the wet states and that the operational definition of field capacity is the soil moisture value at which K reaches some low value at which drainage becomes unimportant, then changes in K_{sat} will translate directly into changes in the field capacity. Furthermore, we note that wet-end drainage is a *fast* process and evapotranspiration is a *slow* process, with respect to changes induced in θ_{rz}. Hence, heuristically, we can think of a short drainage period followed by a long evaporative period, in each interstorm period. Changes in K_{sat} will affect the duration between cessation of rainfall and the onset of pure evaporative control on the trajectory of soil moisture. Perhaps more importantly, through its impact on field capacity, changes in K_{sat} will translate into changes in the θ_{rz} state at the start of the slow evaporative process. Hence, the entire modeled dry-down series of $\theta_{rz}(t)$ will be shifted up or down depending on the direction of the bias in K_{sat}. This is due to the temporally integrative role of the drying process. This

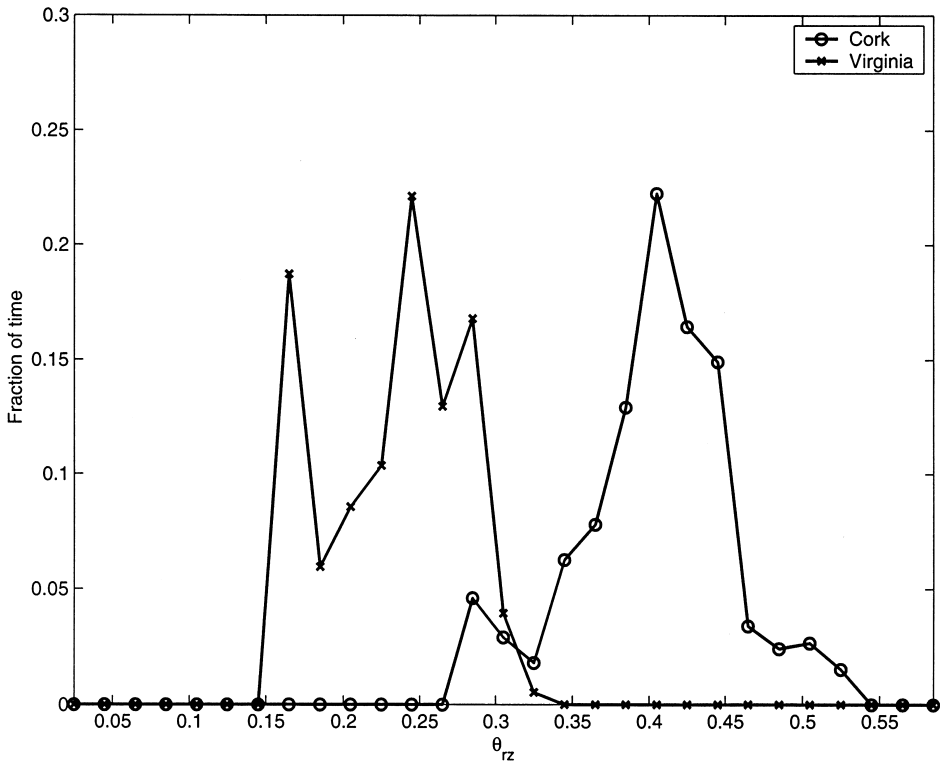

Fig. 3. Frequency distributions of measured soil moisture (from Fig. 1) at the two field sites.

structural impact of drainage on $\theta_{rz}(t)$ is now contrasted with the effects of water-limited transpiration.

Following the short drainage period evapotranspiration progresses at an energy-limited rate until the soil dries to θ_{lim}, below which the rate of water loss is limited by soil moisture status until it ceases at θ_{wilt}. Hence, the particular values of θ_{lim} and θ_{wilt} affect the rates of transpiration, and hence the trajectory of θ_{rz}, only for the range of soil moisture values below θ_{lim}. If storms typically return θ_{rz} to its field capacity or above, then the memory of θ_{lim} is lost following such a storm until the system once again reaches drier conditions. Therefore, the controls of soil moisture on transpiration affect predominantly the dry-end of the soil moisture distribution, whereas the controls of soil moisture on drainage affect the position of the entire distribution. We proceed now to explore the relevance of these hypotheses through paired analyses of measured and modeled time series of soil moisture at each of the wet and dry sites. Since it is rare for the soil moisture values to actually reach θ_{wilt}, we operate with a prescribed θ_{wilt} and explore the effects of θ_{lim}.

4. Results and discussion

The measured time series of θ_{rz} for the Virginia LTER and Cork sites are shown in the top and bottom panels of Fig. 2, respectively. The drought that Virginia was experiencing during the summer of 1998 is apparent from the extended dry-down. Cork, on the other hand, received regular precipitation events and one dry period of nearly 20 days (an uncommon event for Ireland). These field data are depicted as frequency distributions in Fig. 3, where it is apparent that the Virginia data set exhibits a bimodal behavior, with the secondary mode evident on the dry-end from drought persistance and the effective cessation of transpiration. The effect of the intense drainage periods marked by the spiked peaks in Fig. 2 for Cork is depicted by

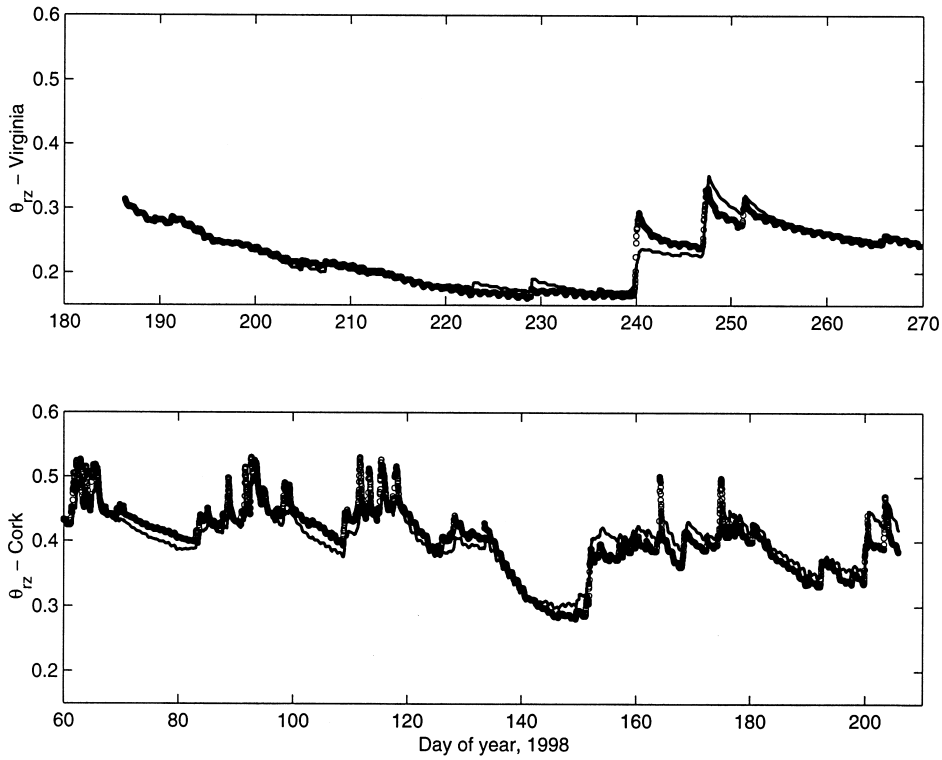

Fig. 4. Comparison of measured (small circles) versus modeled root-zone soil moisture (line) time series for the Virginia (top) and Cork (bottom) field sites.

the heavy wet-end ($0.46 < \theta_{rz} < 0.55$) tail of the frequency distribution for Cork. The value of θ_{rz} associated with the onset of drying (i.e. the wet-end of the distribution) is defined largely by K_{sat}. The extent to which the distribution can extend toward the dry-end is controlled by the θ_{lim} and θ_{wilt} parameters, in concert with the hydroclimatic conditions.

The LSM was used with the measured atmospheric

Table 1
Key parameters used in the land surface model (fit 1:1 from analysis of modeled-versus-measured scatter plots as in Figs. 4 and 5; obs. — approximate value from field observations)

Parameter	Virginia		Cork	
	Value	Source	Value	Source
b	5.47	Murray (2000)	4.38	Texture
K_{sat}	4.0×10^{-6} ms^{-1}	Fit 1:1	2.4×10^{-7} ms^{-1}	Fit 1:1
f_v	0.85	Obs.	1.0	Obs.
$r_{s,min}$	150 sm^{-1}	Following the approach of Ben-Mehrez et al. (1992)	150 sm^{-1}	Following the approach of Ben-Mehrez et al. (1992)
θ_{lim}	0.24	Fit 1:1	0.25	Fit 1:1
θ_{wilt}	0.08	Fit 1:1	0.08	–
z_{om}	0.02 m	Brutsaert (1982)	0.03 m	Brutsaert (1982)
z_{os}	z_{os}/7.4	Brutsaert (1982)	z_{os}/7.4	Brutsaert (1982)

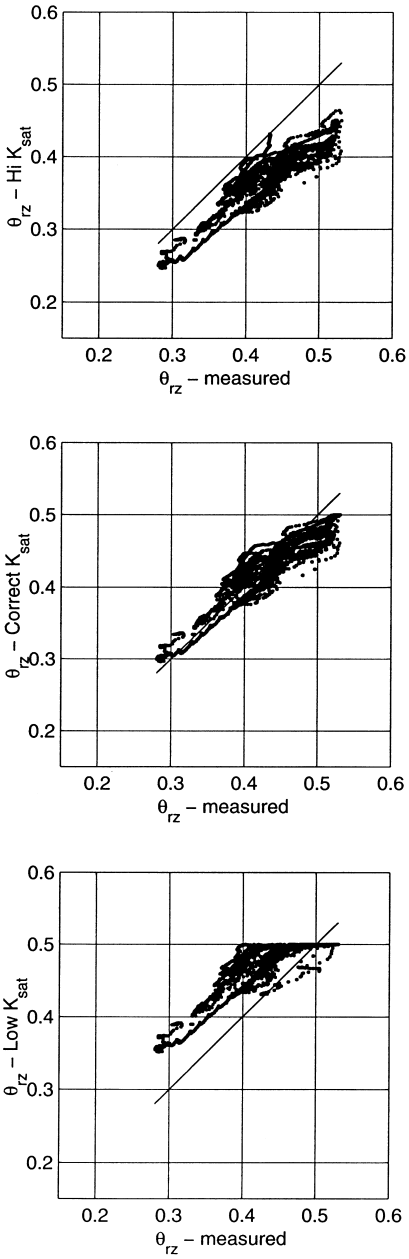

Fig. 5. Comparison of predicted soil moisture to measured soil moisture under three alternative magnitudes of K_{sat} for the wet site (Cork). The top panel is for $5K_{sat}$, the middle is for K_{sat}, and the bottom is for $K_{sat}/5$, where K_{sat} refers to the site-specific value listed in Table 1. Note that the 1:1 lines are shown to mark perfect agreement.

forcing time series to predict fluxes and surface states through the duration of each experiment. The measured and modeled time series of θ_{rz} are plotted in Fig. 4, where we note excellent agreement for the full range of wet and dry excursions. We do not show surface temperature and fluxes of water and energy, as they are outside the scope of the study, but they too were in good agreement to measurements, where available. The soil, vegetation, and bulk surface parameters used in the LSM are listed in Table 1 along with the means of estimating the parameters. Note that the critical parameters K_{sat} and θ_{lim} were defined readily from joint evaluation of modeled and measured time series, as discussed next. In the following analysis, we evaluate the effects of K_{sat} on time series of θ_{rz} using the Cork data set (wet), which is heavily impacted by drainage, and we evaluate the effects of θ_{lim}, using the Virginia data set, which experiences plant water stress.

Overestimates (underestimates) of K_{sat} will result in universal underestimates (overestimates) in the modeled θ_{rz} time series, over the full range of moisture conditions. The logic for this was outlined above. Here we show how a mis-specification of K_{sat} in an LSM affects the predicted series of θ_{rz}, as compared to measured values for the Cork site. In Fig. 5 we compare three sets of predicted soil moisture time series to the single set of measurements: Case 1 (middle panel) uses the correct K_{sat} value as listed in Table 1, Case 2 (top panel) uses K_{sat} increased by a factor of 5, and Case 3 (bottom panel) uses a value decreased by a factor of 5. A factor of 5 is not extreme for saturated conductivities, which typically vary from soil to soil by orders of magnitude. The plateau of the scatter plot in Case 3 is due to the lack of drainage, thus maintaining wet conditions, which in turn yield ponding and surface runoff, as the soil moisture is not allowed to exceed saturation. This point is examined in more depth later. Fig. 5 shows, qualitatively, that a biased estimate of K_{sat} tends to yield a bias in predicted θ_{rz} that is uniform over the range of encountered moisture conditions. This is observed quantitatively as a shifted 'intercept' in a linear fit of predicted-versus-measured soil moisture and observed qualitatively as a stationary offset in the predicted time series for the range of moisture values under evaporative control. We computed a robust measure of offset between the predicted and measured

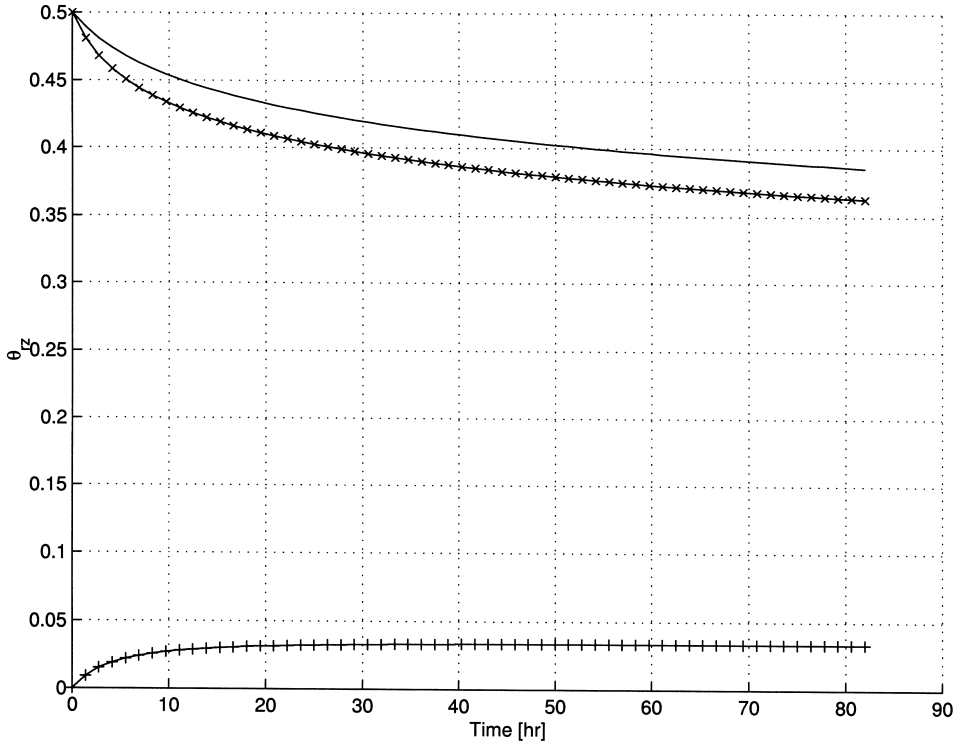

Fig. 6. The black line is an analytical dry-down trajectory, the line with 'x' marks is also a corresponding trajectory with K_{sat} defined to be a factor of 3 higher. The line with '+' marks is the plot of the predicted difference between the lines from the first-order Taylor series analysis (8).

soil moisture distributions. The average bias is computed simply as the time-average of a series derived by subtracting the measured soil moisture (for a given case) from the predicted soil moisture. The average biases for the three cases are: Case 1 (K_{sat} from Table 1) bias = O 10^{-4}, Case 2 ($5K_{sat}$) bias = -0.054, Case 3 ($K_{sat}/5$) bias = 0.052. Given that the time-average of the measured root-zone soil moisture for Cork was 0.40, we see that a factor of 5 error in K_{sat} yields a nearly stationary bias in the θ_{rz} time series that is approximately 13% of the mean. This bias is symmetrical with respect to over- and underestimates of K_{sat} for the moderate range of parameter values and the particular climate considered in this example. Later in this section we demonstrate behavior over a broader range of K_{sat} and differing precipitation intensities.

To explore the apparent stationarity in the bias of root-zone soil moisture resulting from mis-specification of K_{sat}, we consider the temporal dynamics of the total water storage in the root zone, as represented by Eq. (1), during dry-down periods between storms (therefore, $P_g = 0$). We restrict analysis to the range of soil moisture values exceeding the threshold value at which evapotranspiration rates become water-limited ($\theta > \theta_{lim}$), such that evaporative losses from the root zone will be independent of the state of the root zone. Hence, we focus on the drainage process to explore the effects of errors in K_{sat} on trajectories (and biases) of θ_{rz}. The root-zone water balance (1) combined with the gravity drainage formulation (4) becomes

$$\frac{\partial \theta_{rz}}{\partial t} = \frac{-K_{sat}}{d_{rz}} \left(\frac{\theta_{rz}}{\theta_{rz,max}} \right)^{2b+3} \tag{6}$$

which is readily integrated from an initially saturated condition at $t = 0$ to provide an analytical representation of the soil moisture at any later time

$$\theta_{rz}(t) = \theta_{rz,max} \left(1 - \frac{K_{sat} t(-2b-2)}{d_{rz} \theta_{rz,max}} \right)^{(1/(-2b-2))} \tag{7}$$

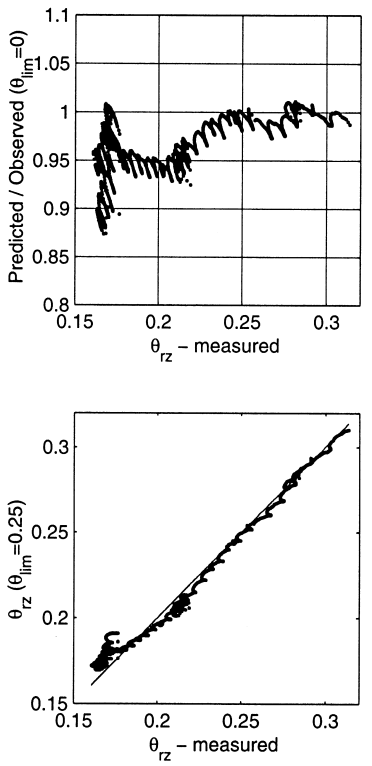

Fig. 7. The top panel shows the ratio of predicted soil moisture to measured soil moisture for a case with no water-limitations on predicted transpiration rates (i.e. $\theta_{lim} = 0$). The bottom panel compares predicted to measured soil moisture, with the modeled transpiration assuming $\theta_{lim} = 0.24$ as identified from inspection of the top panel.

We now seek to demonstrate that an incremental difference in K_{sat} will yield a relatively stationary bias in the time series of θ_{rz}. From a first-order Taylor series expansion and differentiation of Eq. (7) we have

$$\Delta\theta_{rz} = \frac{\partial\theta_{rz}}{\partial K_{sat}}\Delta K_{sat} = \frac{-t\Delta K_{sat}}{d_{rz}}\left(1 - \frac{K_{sat}t(-2b-2)}{d_{rz}\theta_{rz,max}}\right)^{((2b+3)/(-2b-2))} \quad (8)$$

We note that for typical b values the exponent is close to -1, such that we may linearize the result to

$$\Delta\theta_{rz} = \frac{-t\Delta K_{sat}}{d_{rz}}\left(\frac{d_{rz}\theta_{rz,max}}{d_{rz}\theta_{rz,max} - K_{sat}t(-2b-2)}\right) \quad (9)$$

By inspection we see that as time progresses and

$$t \gg \frac{d_{rz}\theta_{rz,max}}{K_{sat}(-2b-2)}$$

the denominator within the brackets approaches

$$-K_{sat}t(-2b-2)$$

and the bias becomes independent of time (i.e. stationary), viz.

$$\Delta\theta_{rz} \approx \left(\frac{\Delta K_{sat}}{K_{sat}}\right)\left(\frac{\theta_{rz,max}}{(-2b-2)}\right) \quad (10)$$

In Fig. 6 we present a pair of trajectories of θ_{rz} based on the analytical drainage solution (7) at two different K_{sat} values (2.4×10^{-6} and 4.8×10^{-6} ms^{-1}). On the same graph we plot the evolution of the bias as predicted by the Taylor series expansion (8). We note that the stationary bias is evident after the early drainage phase, thus supporting the validity of the linearization approximation adopted above. From the above analysis we would expect that the stationarity should be valid for $t \gg 5$ h, which does appear to be the case. The addition of evaporative losses to the above solution should not induce a bias as the non-soil-controlled evaporative losses are not expected to vary systematically with soil water status. We conclude from this analysis that the mis-specification of K_{sat} leads to the development of a bias during the early drainage process, which is maintained at a stationary magnitude through subsequent drainage and evaporation until the soil moisture reaches the limiting value with respect to evaporation. Below the threshold at which soil controls on evapotranspiration become important, the bias will be dampened through time.

In contrast to the effects of K_{sat}, the impact of θ_{lim} on θ_{rz} is primarily on the dry-end of the distribution. We demonstrate this by comparing measurements with predictions that were made with no water-limitation imposed on transpiration (i.e. $\theta_{lim} = 0$). The ratio of θ_{rz} predicted for the no water-limitation case to measured θ_{rz} is shown in the top panel of Fig. 7 for the Virginia site. We focus here on the relevant period beginning at the start of the experiment and ending on day 238. The departure of the ratio from unity is apparent at soil moisture values less than 0.24. This provides a simple assessment of $\theta_{lim} = 0.24$ (approximately). Using this value we generate predicted time

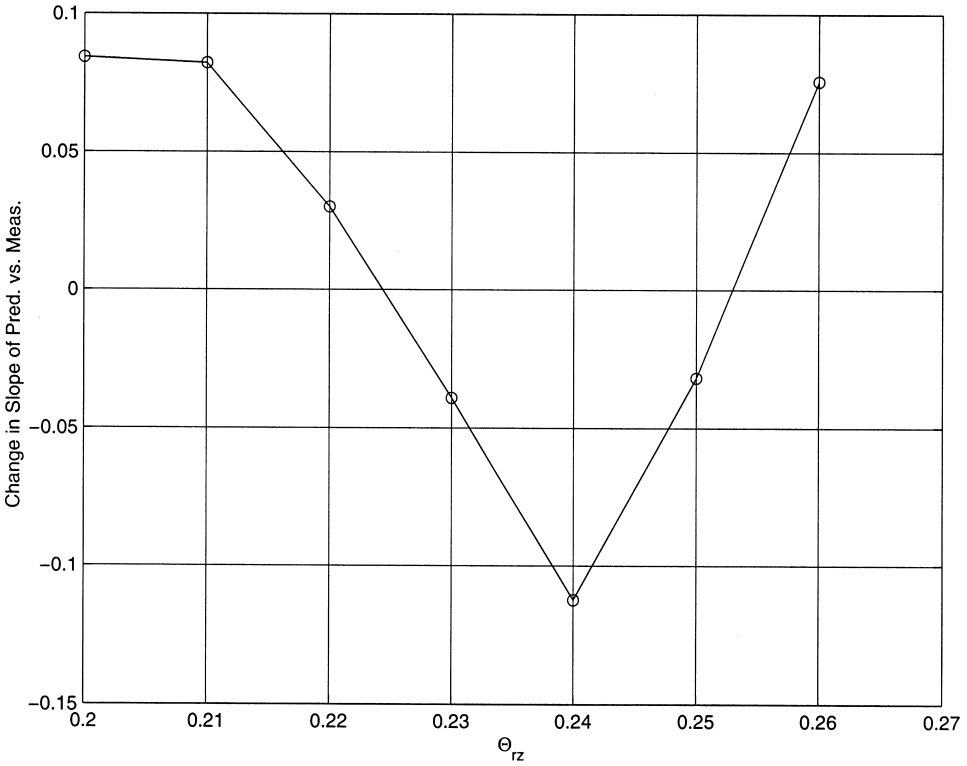

Fig. 8. Rate change in regressed slope of predicted (with $\theta_{lim} = 0$) versus measured soil moisture between adjacent, narrow regression windows ($\Delta\theta_{rz} = 0.03$) plotted against soil moisture value marking the division between the windows.

series of θ_{rz} and compare them to measured values in the bottom panel of Fig. 7, with excellent agreement.

We now demonstrate a more objective means of identifying the location of θ_{lim}. The predicted time series of θ_{rz} for the Virginia site, obtained using $\theta_{lim} = 0$, is evaluated against the measured time series of θ_{rz} from the TDR. A pair of moving windows are used to provide regressed slopes from adjacent narrow bands of the predicted-versus-measured values. The windows each represent a range along the measured axis of width $\Delta\theta_{rz} = 0.03$. These windows are shifted along the measured axis in increments of 0.01 and the difference between the slope in the high-side window and the slope in the low-side window is computed and graphed against measured soil moisture. The results of this analysis are shown in Fig. 8. The most negative value on the graph represents θ_{lim}, as this is where the predicted series changes from under-predicting to matching the measured soil moisture. Hence, at this point, on a graph of predicted (Y axis) versus measured (X axis) soil moisture the slope decreases from a steep value to unity.

In summary, the presence of a bias in predicted-versus-measured soil moisture over the full range of conditions is evidence of an incorrect K_{sat}, and analysis of this bias can lead to an estimate of the appropriate K_{sat} value. A departure on the predicte-versus-measured scatter plot that is local to the dry-end can guide the estimation of θ_{lim}. The impact on the statistical structure of soil moisture from these two process-parameters, which were found to be the critical links in the skill of LSMs (Koster and Milly, 1997) is seen in the frequency distribution comparison shown in Fig. 9 (Cork) and Fig. 10 (Virginia).

Table 2 contrasts several important statistical measures of the structure of the distributions of θ_{rz} across the three cases employed above, subject to the hydrometeorological conditions prevailing during the field measurement campaigns. It is apparent that the value of K_{sat} used in an LSM primarily affects the

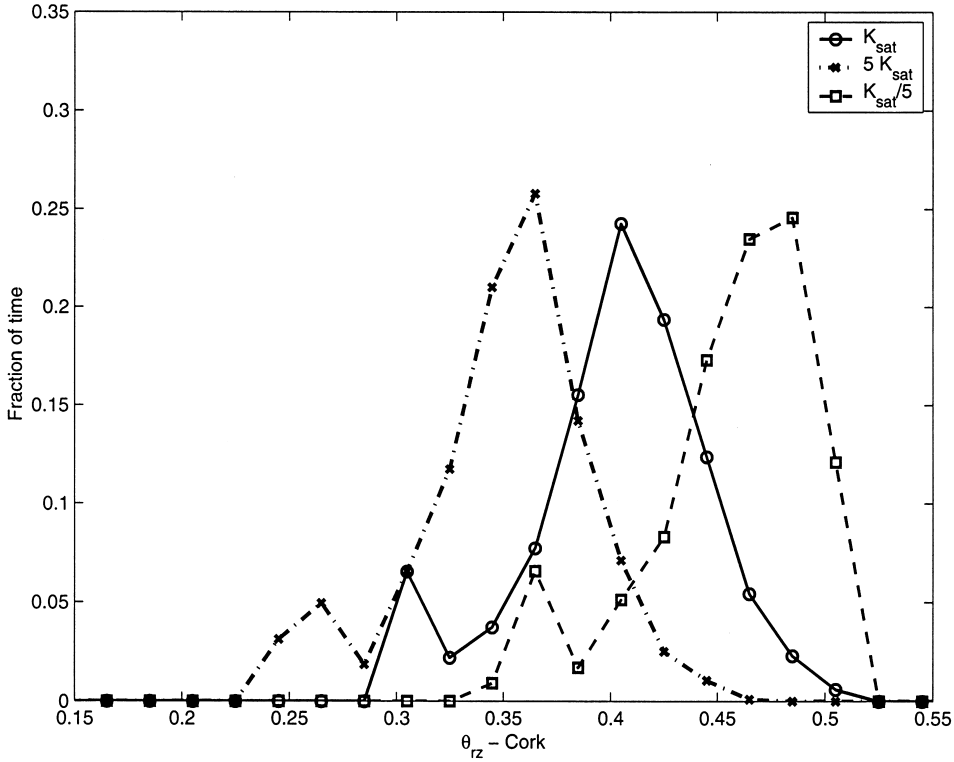

Fig. 9. Frequency distributions of predicted time series of root-zone soil moisture for the Cork site, under the three K_{sat} scenarios as in Fig. 4.

temporal mean of the θ_{rz} distribution for modest changes in K_{sat} about the correct value. There are moderate influences on the variances of the distributions (see Fig. 9). More clear, in this example, is the depiction of how an excessively low K_{sat} will maintain high moisture values that, through interactions with the hard bound at the saturation moisture content, lead to an increasingly negative skewness in the structure of the θ_{rz} distribution. Physically, this is due to the reduction of drainage, which acts to maintain saturated conditions during wet periods and to provide ample moisture availability to support long dry-down excursions during extended periods of heavy transpiration between storms.

The effect of the θ_{lim} on the structure of the time series is shown graphically in Fig. 10 and with quantitative measures in Table 2. Fig. 10 is empirical evidence in support of an earlier statement regarding the general restriction of impacts from water-controls on transpiration to the dry-end of the distribution. The position of the wet-end of the distribution is maintained by K_{sat}, and the shapes of the two distributions are nearly identical between the wet- to mid-ranges. In contrast to the data from Cork, here the distribution is positively skewed, constrained on the dry-end by θ_{lim} and θ_{wilt}, with occasional far excursions into the wet-end. In this case, the effect of a lower θ_{lim} is to allow greater dry-end excursions, thus adding symmetry (or offset) to some of the positive excursions and reducing the skewness of the distribution. The flatness factors reported in Table 2 are a measure of the heaviness of the tails of the distribution. For context, we note that a Gaussian distribution has (by definition) a flatness factor of 3.0. Hence, the Cork soil moisture series has a structure closer to Gaussian than does the Virginia series, with respect to flatness (or heaviness of tails).

To explore further the impacts on the structure of the distributions from the degree of interaction with moisture limits (e.g. saturation), we present results from nine simulation runs using a wider range of K_{sat} values in Fig. 11. In the top panel, it is evident

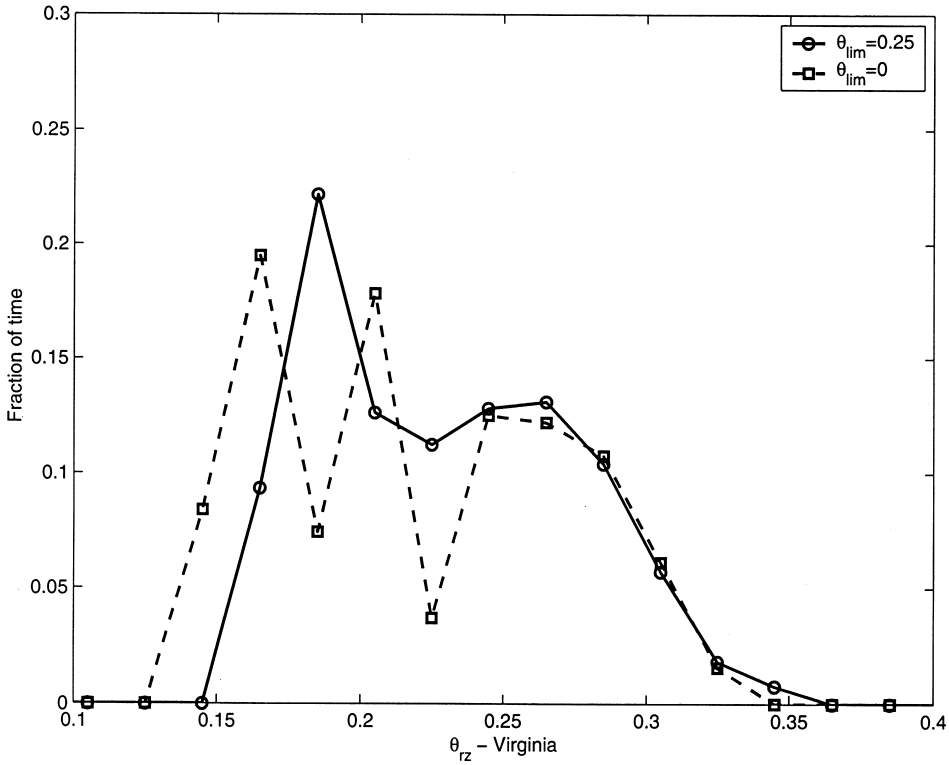

Fig. 10. Frequency distributions of predicted time series of root-zone soil moisture for the Virginia site, under the two θ_{lim} scenarios.

that the absolute bias between predicted and measured moisture at Cork has a global minimum at the selected K_{sat} value (as marked by the arrow). In the middle panel we see that decreases in K_{sat} yield substantially lower variances in θ_{rz} as the bound at θ_{sat} limits the wet-end tail of the distribution. However, increases in K_{sat}, over a fairly wide range above the threshold value, have a relatively minor influence on the variance, as the distributions are shifted toward the drier end with only minor changes in shape and width (e.g. see Fig. 9). The role of the upper bound is also clear on the skewness (bottom panel of Fig. 11). Wetter distributions, from lower K_{sat} values, have increasingly assymetrical tails as quantified by the increasingly negative skewness values. The skewnesss is insensitive to shifts toward drier distributions resulting from further increases in K_{sat} above the threshold. It is important to note that these results are all subject to the particular precipitation forcing and evaporative demand. The hydraulic conductivity only defines the soil's proclivity to retain or drain water. See Castelli et al. (1996) for an analytical exploration of the memory and feedback effects of these processes on subsequent precipitation patterns.

Table 2
Impacts of soil moisture controls on drainage and transpiration on several measures of the statistical structure of the root-zone soil moisture. Note that the skewness and flatness measures are the normalized third and fourth central moments of the distribution, respectively

	Mean	Variance	Skewness	Flatness
Cork: K_{sat}	0.40	0.0018	−0.58	3.27
Cork: $5K_{sat}$	0.35	0.0017	−0.56	3.32
Cork: $(1/5)K_{sat}$	0.45	0.0014	−1.12	3.64
Virginia: $\theta_{lim} = 0$	0.22	0.0025	0.17	1.79
Virginia: $\theta_{lim} = 0.25$	0.23	0.0020	0.34	2.03

We examine the role of precipitation in defining the position of the thresholds of the variance and skewness sensitivities to K_{sat} in Fig. 12. The measured precipitation time series ($P(t)$) is perturbed to provide two alternative precipitation time series ($2P(t)$ and

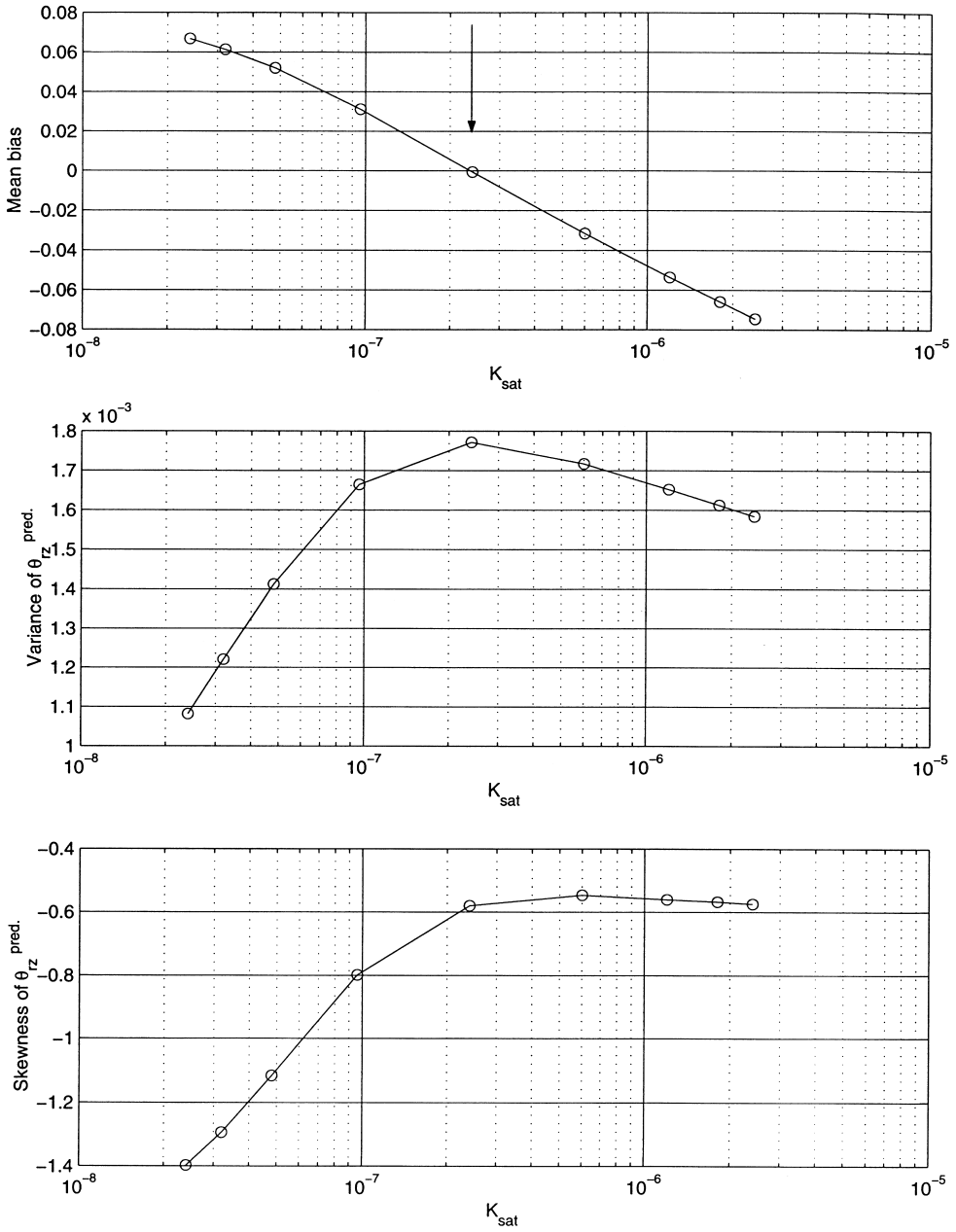

Fig. 11. Results from analysis of nine cases of predicted soil moisture time series for Cork ($K_{sat}/10$, $K_{sat}/7.5$, $K_{sat}/5$, $K_{sat}/2.5$, K_{sat}, $2.5K_{sat}$, $5K_{sat}$, $7.5K_{sat}$, and $10K_{sat}$). In the top panel, the average bias between the predicted time series and the measured series are plotted against the K_{sat} value used in the LSM. In the middle and bottom panels, the variances and skewnesses of the predicted time series are shown, respectively.

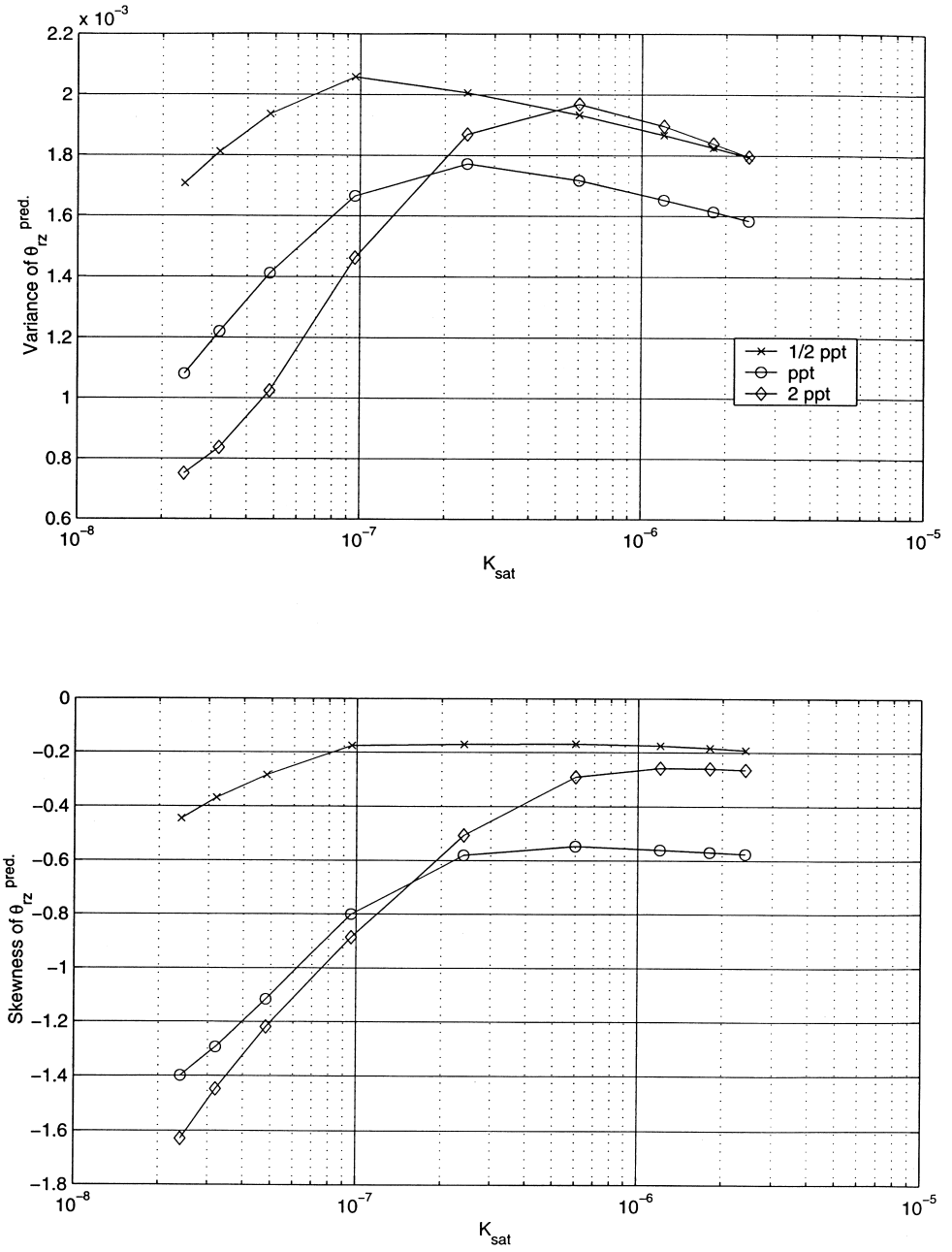

Fig. 12. As in Fig. 9, the variances and skewnesses of predicted time series are shown for Cork, using the same series of K_{sat} values; however, three different precipitation time series are used to force each K_{sat} case. The circles denote results obtained using the measured Cork precipitation series, the ×s denote results from a series with the precipitation intensities decreased by 50%, and the diamonds mark results using a doubled precipitation intensity.

$0.5P(t)$). These scenarios simply explore changes to the precipitation intensities, not the distribution of occurrence. Note from Fig. 12 that, as should be expected, increasing precipitation causes the threshold K_{sat} to shift toward higher values. This is because greater drainage is required under the more intense precipitation to avoid significant interaction with the saturation bound on the θ_{rz} distribution. Not as directly intuitive is the crossing of the lines in Fig. 12 between low and high conductivities. We see that with a highly conductive soil the variance of soil moisture increases for both increases and decreases in precipitation intensities. Furthermore, for the high K_{sat} cases the magnitude of the skewness is reduced for both increasing and decreasing precipitation intensities. In the intense precipitation case, the increased symmetry is due to a reduction in dry-end excursions. In the reduced precipitation case, the increased symmetry is simply due to less interaction with the wet-end bound.

5. Conclusions

Much of the disparity in water and energy balance calculations across land surface models (or SVAT models) has been shown to be due to differences among models in their assumed relationships relating drainage to soil moisture and relating transpiration to soil moisture (Koster and Milly, 1997). Through the analysis of soil moisture data sets from two field experiments and the use of a simple model of root-zone soil moisture evolution, we demonstrated distinctly different impacts to the structure of soil moisture from drainage than from water-limitation on transpiration.

From analysis of a data set collected under relatively wet conditions (Cork, Ireland) we demonstrated that a bias in the estimated saturated conductivity induced a stationary bias in the predicted soil moisture time series. A factor of 5 increase in K_{sat} induced a stationary decrease in soil moisture for the Cork site equal to 13% of the measured mean, a factor of 5 decrease induced a stationary increase in soil moisture equal to 13% of the measured mean. Hence, we conclude that a relatively stationary bias in predicted soil moisture time series (compared to measured values) can be considered evidence of a bias in the assumed value of K_{sat}. Consequently, minimization of the bias provides a simple means of estimating K_{sat}. An analytical relationship between the bias in K_{sat} and resulting bias in moisture was derived. The predictions that result from this approach are encouraging when compared to more rigorous inversion techniques that require more elaborate measurement campaigns (e.g. Cahill et al., 1999).

The biased K_{sat} estimates were also shown to induce changes to the variance and skewness of the root-zone soil moisture time series when shifts in the moisture distribution are severe enough to induce significant impacts from a firm bound (e.g. θ_{sat}). Given the direct interaction between soil moisture and energy partitioning at the land surface, related changes to the temporal structure of latent and sensible heat fluxes are likely to be induced.

The relatively dry hydrometeorological conditions of the Virginia data set provided an opportunity to explore water-stress effects on transpiration. We demonstrated that changes in the assumed moisture content at which transpiration becomes limiting affect predominantly the dry-end of the soil moisture distribution. This is due to the tendency of rainfall events to remove memory of the antecedent dry state. Hence, focused analysis of a localized dry-end departure of predicted soil moisture time series from the measured series provides the means to identify the moisture state at which transpiration becomes limiting. Biases in the limit value lead to changes in the variance of soil moisture, which will likely translate into artificially high or low temporal variances in latent and sensible heat exchanges to the atmosphere.

With the parameters that describe the key moisture losses deduced from the approach described above, soil moisture time series were predicted and found to agree closely with the measured series. It is encouraging that the processes that are known to offer the greatest uncertainties in LSM efforts are deduced readily from simple TDR measurements of soil moisture over limited-duration experiments. There is hope that with continued improvements in the remote sensing of soil moisture we may, in the future, derive spatial coverage of temporal structure of soil moisture, from which model treatment of soil moisture controls on drainage and transpiration can be constrained practically.

Acknowledgements

The Virginia portion of this work was supported by the US Geological Survey under a Regional Competitive Grant #1434-HQ-96-GR-02703, The National Science Foundation's LTER program under grant #IBN-9411974, and NASA's New Investigator in the Earth Sciences Program under grant #NAG5-8670. The Cork portion of the work was funded by the European Union Inco-Copernicus Project #IC15-CT98-0120. The Virginia data set was made possible through the field efforts of Laura Murray and Scott Dusterhoff.

References

Avissar, R., Peilke, R.A., 1991. The impact of plant stomatal control on mesoscale atmospheric circulations. Agric. For. Meteorol. 54, 353–372.

Belair, S., LaCarrere, P., Noilhan, J., Masson, V., Stein, J., 1998. High-resolution simulation of surface and turbulent fluxes during HAPEX-MOBILHY. Mon. Weather Rev. 126, 2234–2253.

Ben-Mehrez, M., Taconet, O., Vidal-Madjar, D., Valencogne, C., 1992. Estimation of stomatal resistance and canopy evaporation during the HAPEX-MOBILHY experiment. Agric. For. Meteorol. 58, 285–313.

Boulet, G., Braud, I., Vauclin, M., 1997. Study of the mechanisms of evaporation under arid conditions using a detailed model of the soil–atmosphere continuum: application to the EFEDA I experiment. J. Hydrol. 193, 114–141.

Brutsaert, W., 1982. Evaporation into the Atmosphere. Kluwer Academic, Dordrecht (299pp.).

Cahill, A.T., Ungaro, F., Parlange, M.B., Nielsen, D., 1999. Combined spatial and Kalman filter estimation of optimal soil hydraulic properties. Water Resour. Res. 35, 1079–1088.

Castelli, F., Rodriquez-Iturbe, I., Entekhabi, D., 1996. An analytical framework for the modeling of the spatial interaction between the soil moisture and the atmosphere. J. Hydrol. 184, 19–34.

Chen, F., Mitchell, K., Schaake, J., Xue, Y., Pan, H.-L., Koren, V., Duan, Q.Y., Ek, M., Betts, A., 1996. Modeling of land surface evaporation by four schemes and comparison with FIFE observations. J. Geophys. Res. 101 (D3), 7251–7268.

Clapp, R.B., Hornberger, G.M., 1978. Empirical equations for some soil hydraulic properties. Water Resour. Res. 14, 601–604.

Cosby, B.J., Hornberger, G.M., Clapp, R.B., Ginn, T.R., 1984. A statistical exploration of the relationship of soil characteristics to the physical properties of soils. Water Resour. Res. 20, 682–690.

Deardorff, J.W., 1978. Efficient prediction of ground surface temperature and moisture, with inclusion of a layer of vegetation. J. Geophys. Res. 83 (C4), 1889–1903.

Delworth, T.L., Manabe, S., 1988. The influence of potential evaporation on the variabilities of simulated soil wetness and climate. J. Clim. 1, 523–547.

Delworth, T.L., Manabe, S., 1989. The influence of soil wetness on near surface atmospheric variability. J. Clim. 2, 1447–1462.

Ek, M., Cuenca, R.H., 1994. Variation in soil parameters: implications for modeling surface fluxes and atmospheric boundary-layer development. Boundary-Layer Meteorol. 70, 369–383.

Entekhabi, D., Rodriquez-Iturbe, I., Castelli, F., 1996. Mutual interaction of soil moisture state and atmospheric processes. J. Hydrol. 184, 3–17.

Famiglietti, J.S., Rudnicki, J.W., Rodell, M., 1998. Variability in surface moisture content along a hillslope transect — Rattlesnake Hill, Texas. J. Hydrol. 210, 159–181.

Famiglietti, J.S., Devereaux, J.A., Laymon, C.A., Tsegaye, T., Houser, P.R., Jackson, T.J., Graham, S.T., Rodell, M., van Oevelen, P.J., 1999. Ground-based investigation of soil moisture variability with remote sensing footprints during the Southern Great Plains 1997 (SGP97) Hydrology Experiment. Water Resour. Res. 35, 1839–1851.

Henderson-Sellers, A., 1996. Soil moisture: a critical focus for global change studies. Global Planet. Change 13, 3–9.

Henderson-Sellers, A., Zang, Z.-L., Dickinson, R.E., 1993. The project for intercomparison of land-surface parameterization schemes. Bull. Am. Meteorol. Soc. 74, 1335–1349.

Henderson-Sellers, A., Mcguffie, K., Pitman, A.J., 1996. The project for intercomparison of land-surface parameterization schemes (PILPS) — 1992 to 1995. Clim. Dynam. 12 (12), 849–859.

Jacquemin, B., Noilhan, J., 1990. Sensitivity study and validation of a land surface parameterization using the HAPEX-MOBILHY data set. Boundary-Layer Meteorol. 52, 93–134.

Kim, C.P., Stricker, J.N.M., 1996. Consistency of modeling the water budget over long time series: comparison of simple parameterizations and a physically based model. J. Appl. Meteorol. 35, 749–760.

Kim, J., Ek, M., 1995. A simulation of the surface energy budget and soil water content over the hydrologic atmospheric pilot experiment-modelisation du bilan hydrigue forest site. J. Geophys. Res. 100 (D10), 20,845–20,854.

Koster, R.D., Milly, P.C.D., 1997. The interplay between transpiration and runoff formulations in land surface schemes used with atmospheric models. J. Clim. 10, 1578–1591.

Kutìlek, M., Nielsen, D.R., 1994. Soil Hydrology. Catena (370pp.).

Mahfouf, J.-F., Noilhan, J., 1996. Inclusion of gravitational drainage in a land surface scheme based on the force–restore method. J. Appl. Meteorol. 35, 987–992.

Murray, L.A., 2000. Dynamics of soil moisture at the VCR/LTER. MS thesis, University of Virginia.

Noilhan, J., Planton, S., 1989. A simple parameterization of land surface processes in meteorological models. Mon. Weather Rev. 117, 536–549.

Noilhan, J., Mahfouf, J.-F., 1996. The ISBA land surface parameterisation scheme. Global Planet. Change 13, 145–159.

Rodriquez-Camino, E., Avissar, R., 1998. Comparsion of three land-surface schemes with the Fourier amplitude sensitivity test (FAST). Tellus 50A, 313–332.

Rodriquez-Iturbe, I., D'Odorico, P., Porporato, A., Ridolfi, L., 1999.

On the spatial and temporal links between vegetation, climate, and soil moisture. Water Resour. Res. 35, 3709–3722.

Shao, Y., Henderson-Sellers, A., 1996. Validation of soil moisture simulation in landsurface parameterisation schemes with HAPEX data. Global Planet. Change 13, 11–46.

Verhoest, N.E.C., Troch, P.A., Paniconi, C., DeTroch, F.P., 1998. Mapping basin scale variable source areas from multitemporal remotely sensed observations of soil moisture behavior. Water Resour. Res. 34, 3235–3244.